Microdomain Morphology in an ABC 3-Miktoarm Star Terpolymer: A Study by Energy-Filtering TEM and 3D Electron Tomography

Kazuhiro Yamauchi, Keiko Takahashi, and Hirokazu Hasegawa*

Department of Polymer Chemistry, Graduate School of Engineering, Kyoto University, Kyoto 615-8510, Japan

Hermis Iatrou and Nikos Hadjichristidis

Chemistry Department, University of Athens, Panepistimiopolis, Zografou 15771, Athens, Greece

Takeshi Kaneko, Yukihiro Nishikawa, and Hiroshi Jinnai

Department of Polymer Science and Engineering, Kyoto Institute of Technology, Goshokaido-cho, Matsugasaki, Kyoto 606-8585, Japan

Toshimitsu Matsui

Sekisui Chemical Co. Ltd., 2-1 Hyakuyama, Shimamoto-cho, Mishima-gun, Osaka 618-8589, Japan

Hideo Nishioka

JEOL Ltd., 1-2-3 Musashino, Akishima, Tokyo 196-8556, Japan

Miyoko Shimizu and Hiromitsu Furukawa

JEOL System Technology Co. Ltd., 1-2-3 Musashino, Akishima, Tokyo 196-8556, Japan

Self-assembled structures in block copolymers have received considerable attention due to their morphological varieties. A great number of morphological studies have been reported, and it was shown that the three-component systems such as ABC linear triblock terpolymers (linear ABC) could form more complex and more intriguing microdomain structures than AB diblock copolymers because of their complex self-assembling mechanisms.[1−7] Although ABC 3-miktoarm star terpolymers (star ABC) also belong to the ABC ternary systems, the reports of their morphology are limited to a small number because of the difficulties in their synthesis.[8−12]

Obviously, star ABC fundamentally differs from linear ABC. For example, linear ABC has two junctions (one between A and B blocks and the other between B and C blocks), and each junction is confined in a narrow interfacial area. On the other hand, in star ABC a single junction point connects the three different blocks, and the junction points are confined on a linear or curved line where the three interfaces (between A and B microphases, between B and C microphases, and between C and A microphases) meet. This difference in the spatial arrangements of the junction points between linear and star ABC may dramatically change their self-assembly and the resulting microdomain structures. Therefore, microdomain morphologies of star ABC cannot be easily imagined, though those of linear ABC are

* Corresponding author: e-mail hasegawa@alloy.polym.kyoto-u.ac.jp.

often similar to those of AB diblock copolymers.[13−16] Dotera et al. investigated the microdomain morphologies of star ABC with the arm-length ratios of 1:1:*x* (*x*: variable) by a computer simulation method and predicted that all three components would form polygonal cylindrical microdomains and that the junction points should be confined on a linear line.[17,18] However, asymmetry in the repulsive interactions among the three components often results in a different morphology from their predictions. For example, Okamoto et al. found a 3D continuous microdomain structure for the star ABC [A: polystyrene, PS; B: poly(*tert*-butyl methacrylate), PTBMA; C: poly(dimethylsiloxane), PDMS] with the arm-length ratio of about 1:1:1,[14] and Sioula et al. found a coaxial cylindrical microdomain structure for the star ABC [A: PS; B: poly(methyl methacrylate), PMMA; C: polyisoprene, PI] with the arm-length ratio of about 1:1.2:1.7.[15] These results suggest that the junction points of star ABC are not always arranged on a linear line, and therefore, it is not appropriate to assume cylindrical microdomain structures for the structure analysis of star ABC. Since the TEM images of star ABC show complex patterns in general, it is dangerous to rely on our experiences in the structure determination of diblock copolymers. Therefore, we employed electron tomography to observe in real space a three-dimensional image of such a complex nanostructure free from a preconception.[19−21]

In this paper we report the three-dimensional microdomain structure of the star ABC composed of PS, PI, and PDMS with the arm-length (M_n) ratio of almost 1:1:1 (PS: 19.5K; PI: 20.7K; PDMS: 19.0K). In this case, strong repulsive interactions among the three different blocks yield a three-phase microdomain structure at room temperature. For observation of its microdomain morphology, we prepared two kinds of specimens for transmission electron microscopy (TEM) by cryo-ultramicrotoming of the sample film cast from toluene solution and then annealed. One is the specimen without staining. Another is the specimen stained with OsO_4. In these specimens, just one phase has a contrast under TEM, and the two specimens give the complementary information. For the observation of the ABC ternary systems, it is desirable to give different contrast to different components on the same image by using selective staining agents. However, it is complicated to display and analyze a 3D image composed of three different contrasts, and it is advantageous to investigate each phase individually. For synchronizing two images with different contrast, we utilized an energy-filtering TEM (EF-TEM).

The methodology of the synthesis of (PI)(PS)(PDMS) 3-miktoarm star terpolymer was based, on one hand, on recent advances in the controlled anionic polymerization of hexamethylcyclotrisiloxane and, on the other hand, on the selective replacement of the chlorines of trichloromethylsilane by the living chains of PI, PS, and PDMS. The linking reaction was monitored by size exclusion chromatography (SEC). The final product was fractionated. The good agreement between the measured PS, PI, and PDMS content by ^{1}H NMR (and UV in the case of PS) and the composition calculated on the basis of the molecular weights of the arms and the total molecular weight of the final products indicate high

degrees of molecular and compositional homogeneity. This is also supported by the narrow molecular weight and compositional distribution obtained by SEC. The details of the synthesis were described elsewhere.[11]

The film specimens were prepared by casting from 7 wt % polymer solution in toluene. The cast film was annealed at 150 °C for 12 h under vacuum. The annealed film specimens were ultramicrotomed with a glass knife under a dry condition at −120 °C using a Reichert Ultracut E ultramicrotome equipped with a cryogenic sectioning unit before staining. Two ultrathin sections were prepared. One was observed as prepared, and the other was stained with the vapor of 2 wt % aqueous solution of osmium tetraoxide (OsO_4) at room temperature for 1 h. The microdomain structures were observed under an energy-filtering transmission electron microscope with a field-emission gun. A JEOL JEM-2010FEF electron microscope equipped with an omega filter was used. The TEM observation was done at the accelerating voltage of 200 kV, and the digital image data were collected using a Gatan slow-scan CCD camera. For electron tomography, a series of 61 images were collected at tilt angles ranging from +60° to −60° in a 2° step with a computer-controlled sample stage. Three-dimensional reconstruction was done with the program developed by JEOL System Technology Co., Ltd. [22]

The results from EF-TEM of unstained and OsO_4-stained ultrathin sections are given in parts a−c and parts d−f of Figure 1, respectively. All TEM pictures shown in Figure 1 were taken at high magnification. At low magnification, we observed many defects (e.g., a microdomain structure exhibiting a triangular pattern), and the size of the regions (grains) as shown in Figure 1 was very small. Figure 1a,d shows the zero-loss ($\Delta E = 0$) images; i.e., they are imaged with the transmitted and scattered electrons having the same wavelength as the incident electron beam. Zero-loss images are similar to the conventional TEM images, but they are superior in resolution and contrast because the energy filter equipped in the microscope eliminates the inelastically scattered electrons, which cause chromatic aberration. Despite no staining applied, Figure 1a has a good contrast due to the Si atoms contained in the PDMS component, but there is no appreciable contrast between the PI and the PS phase in the zero-loss image. The dark rectangular or square areas observed in Figure 1a were attributed to the PDMS microdomains. However, a closer observation suggests that the corners of the rectangles or squares were truncated, suggesting that the PDMS microdomains may have an octagonal shape. The bright areas should be composed of PS and PI microdomains.

The image of the OsO_4-stained specimen as shown in Figure 1d is quite different from that of the unstained specimen in Figure 1a and exhibits a complex pattern with dark areas of a shape of St. Andrew's cross aligned on a square lattice. A similar pattern has been reported by Hückstädt et al.[12] Evidently, the dark areas of the PDMS microdomains in Figure 1a do not match the bright areas in Figure 1d. It implies that the bright areas in Figure 1d are composed of PS and PDMS microdomains and that the three components, PI, PDMS, and PS, form the microdomains independently. In fact, a closer observation of Figure 1d reveals three kinds of areas: the cross-shaped dark area stained by OsO_4, the bright area adjoining on the concaved sides of OsO_4 stained PI microdomains, but
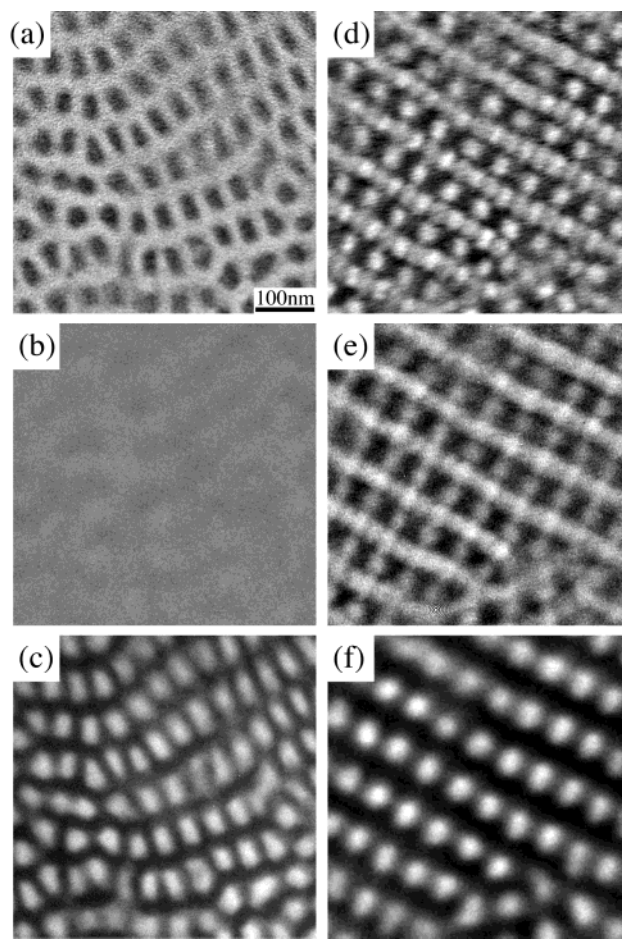

Figure 1. EF-TEM images of (PI)(PS)(PDMS) 3-miktoarm star terpolymer: (a) to (c) are the images of the unstained specimen, and (d) to (f) are the images of the OsO_4-stained specimen. (a) and (d) are the images taken at $\Delta E = 0$ eV, (b) and (e) at $\Delta E = 110$ eV, and (c) and (f) at $\Delta E = 230$ eV. The images are obtained from the same area for each series.

of the dark area, and the less-bright area in contact with the ends of the cross shapes of the dark area.

In the case of the OsO_4-stained specimen, only PI microdomains are stained by OsO_4 and contain Os atoms while PS and PDMS microdomains remain unstained. However, PDMS contains Si atoms as its component. Therefore, the contrast observed in the zero-loss image should be the darkest for the PI microdomains containing Os atoms, less dark for the PDMS microdomains containing Si atoms, and the brightest for the PS microdomains consisting of only C and H atoms. Though such contrast seems to be observed to some extent, the contrast between the PDMS and the PS microdomains is too weak to distinguish the two phases in Figure 1d. Probably, the contrast given to the PI microdomains by Os atoms is too strong to appreciate the contrast between the PDMS and the PS microdomains in this particular case. This result well accords with our previous report.[23] Moreover, it should be noted that the observation of less-dark (gray) area cannot be an immediate proof of the PDMS microdomains because some complex structures such as bicontinuous structures always show variable contrast in the projected images due to the overlap of stained and unstained microdomains in the thickness of the specimens. Consequently, we are sure that the darkest areas in Figure 1d correspond to the OsO_4-stained PI microdomains, but

we cannot distinguish the PS and the PDMS microdomains in the bright areas.

In EF-TEM, element mapping, e.g., via the three-window method,[24] is a common technique to distinguish one component from another if the constituent elements are different for the two components. The image can be formed with the electrons inelastically scattered by a particular element because the amount of ionization energy loss depends on the binding energy of the atomic shell, which is different for different elements. Therefore, Si mapping together with the zero-loss image in the same OsO_4-stained specimen seems to be useful to distinguish the PI and the PDMS microdomains. However, it is not so easy according to our experience. Inelastic scattering intensity except for that from C atoms is very weak for polymers because of the small content of heteroatoms in ordinary polymer samples, and the contrast given by Os atoms is dominant. Consequently, Si mapping was not possible for the OsO_4-stained specimen in our case. Therefore, we chose a different approach from Si mapping.

In such a case, it is convenient to utilize the energy-loss images, which are formed with the inelastically scattered electrons by the specimens. The details of the technique will be described elsewhere.[25] The energy-loss image of the unstained specimen at $\Delta E = 110$ eV corresponding to the same area as Figure 1a is shown in Figure 1b. Though the image was taken in focus, it shows no contrast. Figure 1c shows the energy-loss image at 230 eV obtained from the same area. Although it shows a pattern similar to that in Figure 1a, the contrast is reversed from Figure 1a; i.e., the dispersed PDMS phase appears bright and the matrix phase dark. These results are easy to understand. At zero loss ($\Delta E = 0$ eV) or small ΔE, the PDMS phase has lower intensity than the background (the matrix composed of the PI and PS phases) and appears dark. The ionization energy for the excitation of inner-shell (K-shell) electrons for Si atoms is 99 eV. Since ΔE dependence of the inner-shell excitation has the form of an edge rather than a peak, the spectrum of electrons inelastically scattered from the PDMS phase shows a sudden increase at $\Delta E = 99$ eV and gradual decrease at $\Delta E > 100$ eV, while the spectra for the other components have monotonic decreases across $\Delta E = 99$ eV. As a result, the PDMS phase, rich in Si atoms, becomes bright at $\Delta E = 99$ eV while the background intensity keeps decreasing. At $\Delta E = 110$ eV when the inelastic scattering intensity of the PDMS phase matches the background intensity, no contrast can be observed (Figure 1b). For ΔE over 110 eV, the contrast between the PDMS phase and the matrix is inverted because the Si−K edge of the PDMS phase keeps the scattering intensity at higher level than that of the background while the background intensity quickly decreases. Consequently, the dispersed PDMS phase appears bright, and the matrix consisting of the PI and PS phases appears dark at $\Delta E = 230$ eV, as shown in Figure 1c.

In contrast to the unstained specimen, nearly the same image as Figure 1d was observed for the OsO_4-stained specimen at $\Delta E = 110$ eV as shown in Figure 1e. On the basis of the observation result for Figure 1b that there is no contrast for the three phases at $\Delta E = 110$ eV, the dark area observed in Figure 1e should be the PI phase stained with OsO_4, while the PDMS and the PS phases, both appearing as the bright area, cannot be clearly distinguished. At $\Delta E = 230$ eV, the area
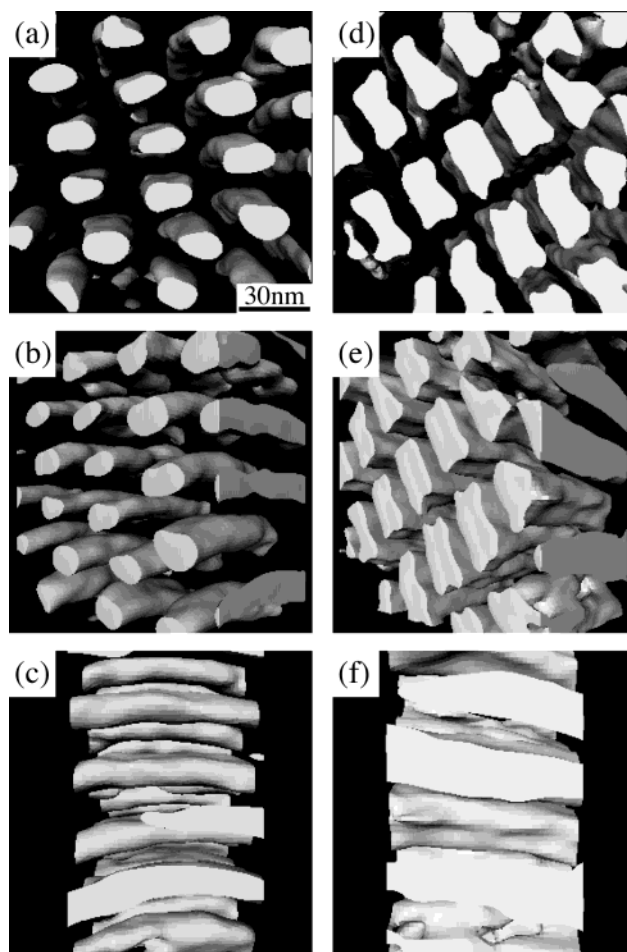

Figure 2. Three-dimensional images of the (PI)(PS)(PDMS) 3-miktoarm star terpolymer obtained by electron tomography: (a−c) unstained specimen; (d−f) OsO_4-stained specimen.

between the concaved sides of the PI microdomains became as dark as the PI phase, and only the area located diagonally on the corners of the PI microdomains could be observed bright as shown in Figure 1f. Since the PDMS phase is observed brighter than the PS phase at $\Delta E = 230$ eV as shown in Figure 1c, the bright area in Figure 1f corresponds to the PDMS phase; i.e., the area located on the corners of the PI phase corresponds to the PDMS microdomains. Consequently, the remaining area located between the concaved sides of the PI microdomains corresponds to the PS phase. The volume fractions calculated with the M_n ratio of the three blocks are 0.302 for PS (density at 25 °C, $d = 1.05$), 0.379 for PI ($d = 0.89$), and 0.319 for PDMS ($d = 0.97$), which are in good agreement with the corresponding area fractions in the micrographs. Thus, we could determine a one-to-one correspondence between the three kinds of areas in the TEM image and the three components. Then, the next step is to find out the 3D shape of each microdomain.

Electron tomography is a very powerful technique for analysis of nanostructures in real space. The details on 3D reconstruction by the back-projection method using a series of tilt images were described elsewhere.[22,25] 3D reconstructed images of the unstained and OsO_4-stained ultrathin sections are given by surface renderings in parts a to c and parts d to f in Figure 2, respectively. All tilt images used for the 3D reconstruction were obtained at $\Delta E = 0$ eV (zero-loss images). The bright solid objects in the 3D images of the unstained specimen
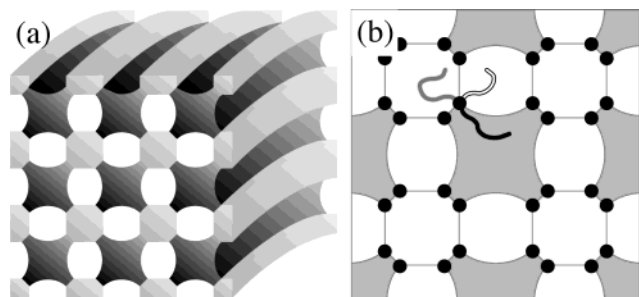
Figure 3. (a) Schematic illustration of the model for the microdomain structure of the (PI)(PS)(PDMS) 3-miktoarm star terpolymer consisting of dark (PI), gray (PDMS), and bright (PS) cylinders with characteristic shapes. (b) A cross-sectional view of the cylinders in (a). The junction points of the star terpolymer are confined on the curved lines and designated by the filled circles in (b).

shown in Figure 2a–c correspond to the PDMS microdomains observed dark in Figure 1a for the unstained specimen. The matrix of the PS and PI phases was removed and appears transparent in the 3D images. Polygonal cylinders (some of them are octagonal) packed in a square lattice were observed in Figure 2a clearly. However, it is obvious that these cylinders are curved collectively into an arc. On the other hand, the objects in the 3D images of OsO$_4$-stained specimen shown in Figure 2d–f correspond to the PI microdomains because the contrast between PS and PDMS phases was too weak to give an influence to the reconstruction of the 3D images. Similar to the PDMS microdomains, the PI microdomains have a cylindrical shape, but their cross section has a shape of a St. Andrew's cross. They are also packed in a square lattice as observed in Figure 2c. The PI cylinders are also bent. The space that remains after removing the PI and the PDMS cylindrical microdomains corresponds to the PS phase. Inevitably, the PS microdomains should also have a shape of bent cylinders packed in a square lattice.

EF-TEM together with electron tomography revealed the 3D microdomain structure of each component of the (PI)(PS)(PDMS) 3-miktoarm star terpolymer. The 3D structural model is shown in Figure 3a. Coexistence of three kinds of cylindrical structures is one of the characteristic features of the microdomain morphology of the star ABC. However, these cylinders were collectively bent into an arc. It is the consequence of confining the central junction points on the arced lines as schematically illustrated in Figure 3a,b. The grain size of the star ABC is extremely small compared with that of liner block copolymers. The junction points are aligned not on straight lines but on arcs, and it may be the reason why the long-range order is missing in the star ABC.

On the other hand, the shapes of the three kinds of cylindrical structures are extremely strange; e.g., the PI phase forms the cylinders having the cross-sectional shape of a St. Andrew's cross. The microdomains with such a strange shape have never been observed in a liner ABC. Hückstädt et al. have reported the similar cross-shaped cylindrical morphology aligned on a square lattice in the star ABC [A: PS; B: polybutadiene, PB; C: poly(2-vinylpyridine), P2VP] with the asymmetric arm-length ratio of about 4.9:1.6:1.0 and 3.1:1.0:2.7.[12] However, our star ABC formed the bent cylinders having the cross-shaped cross sections despite the almost symmetric arm length.

Microdomain morphology in an as-cast specimen of an ABC 3-miktoarm star terpolymer is affected by the casting solvent and the casting process because a nonselective solvent for the three different component polymers usually does not exist. Therefore, we employed the specimen annealed at 150 °C for 12 h under vacuum in this work. However, we are not sure whether the observed structure in this study was the equilibrium morphology. Anyway, the unique morphology observed in this study must be the consequence of asymmetric interactions among the three component polymers.

Dotera et al. predicted that a star ABC with the arm-length ratios of 1:1:1 would form hexagonal cylindrical microdomains exhibiting a honeycomb pattern by computer simulation assuming equal interactions among the three components.[17] In their case, the area of the three kinds of interfaces (interfaces between PI and PS, between PS and PDMS, and between PDMS and PI) must be equal. In our case, despite the arm-length ratios of nearly 1:1:1, three kinds of cylinders packed in a square lattice have different contact area, suggesting that the interactions among the three components are asymmetric.

The solubility parameter increases in the order of PDMS, PI, and PS, and the strongest repulsive interaction arises between PS and PDMS in this terpolymer. Therefore, PS tends to prevent the contact with PDMS, whereas the three components have to adjoin each other due to the star architecture of the molecule. To minimize the interfacial energy, the system would minimize the interfacial area between PS and PDMS (interface between black and gray regions in Figure 3). However, on the other hand, the PS microdomains must keep their inherent volume. Consequently, the PDMS phase forms the octagonal–cylindrical microdomain, and it minimizes the contact area with the PS phase. To keep its inherent volume, the PS phase expands the interfacial area with the PI phase, resulting in the concaved sides of the PI cylindrical microdomains with the cross-shaped cross section. Since fundamentally there are no junction points on the interface except for the intersection of the three interfaces in the case of star ABC (illustrated in Figure 3b), it must be easier for star ABC to expand and bend the interface than linear block copolymers, which have junction points on the interface. Moreover, the interfaces between the PDMS and the PS phases were observed darker than these two phases in some TEM images as shown in Figure 1d,e. This result suggests that some PI chains might exist in the interface between the PDMS and the PS phases, which is possible only for star ABC because there are no junctions in the interface. Consequently, the PI chains prevent from the strongest repulsive interaction between the PS and the PDMS phase. A more desirable situation is that the PS and the PDMS phase are diagonally arranged and do not adjoin each other in the square lattice. However, diagonally arranged were the PI and the PDMS phases in our star polymer. These results suggest that packing of the three kinds of cylinders depends on the composition of the terpolymer. Asymmetric interactions among the three components give a great influence on the microdomain morphology of star ABC; i.e., the junction points fall on the arcs where the three kinds of curved interfaces meet, and the frustrated microdomain structure of the bent cylinders with the strange cross sections resulted.

References and Notes

(1) Shibayama, T.; Hasegawa, H.; Hashimoto, T.; Kawai, H. *Macromolecules* **1982**, *15*, 274.
(2) Kudose, I.; Kotaka, T. *Macromolecules* **1984**, *17*, 2325.
(3) Mogi, Y.; Mori, K.; Matsushita, Y.; Noda, I. *Macromolecules* **1992**, *25*, 5412.
(4) Stadler, R.; Auschra, C.; Beckmann, J.; Krappe, U.; Voigt-Martin, I.; Leibler, L. *Macromolecules* **1995**, *28*, 3080.
(5) Breiner, U.; Krappe, U.; Thomas, E. L.; Stadler, R. *Macromolecules* **1998**, *31*, 135.
(6) Tanaka, Y.; Hasegawa, H.; Hashimoto, T.; Ribbe, A.; Sugiyama, K.; Hirao, A.; Nakahama, S. *Polym. J.* **1999**, *31*, 989.
(7) Abetz, V.; Goldacker, T. *Macromol. Rapid Commun.* **2000**, *21*, 16.
(8) Iatrou, H.; Hadjichristidis, N. *Macromolecules* **1992**, *25*, 4649.
(9) Fujimoto, T.; Zhang, H.; Kazama, T.; Isono, Y.; Hasegawa, H.; Hashimoto, T. *Polymer* **1992**, *33*, 2208.
(10) Sioula, S.; Tselikas, Y.; Hadjichristidis, N. *Macromolecules* **1997**, *30*, 1518.
(11) Bellas, V.; Iatrou, H.; Hadjichristidis, N. *Macromolecules* **2000**, *33*, 6993.
(12) Hückstädt, H.; Göpfert, A.; Abetz, V. *Macromol. Chem. Phys.* **2000**, *201*, 296.
(13) Hadjichristidis, N.; Iatrou, H.; Behal, S. K.; Chludzinski, J. J.; Disko, M. M.; Garner, R. T.; Liang, K. S.; Lohse, D. J.; Milner, S. T. *Macromolecules* **1993**, *26*, 5812.
(14) Okamoto, S.; Hasegawa, H.; Hashimoto, T.; Fujimoto, T.; Zhang, H.; Kazama, T.; Takano, A.; Isono, Y. *Polymer* **1997**, *38*, 5275.
(15) Sioula, S.; Hadjichristidis, N.; Thomas, E. L. *Macromolecules* **1998**, *31*, 5272.
(16) Sioula, S.; Hadjichristidis, N.; Thomas, E. L. *Macromolecules* **1998**, *31*, 8429.
(17) Dotera, T. *Phy. Rev. Lett.* **1999**, *82*, 105.
(18) Gemma, T.; Hatano, A.; Dotera, T. *Macromolecules* **2002**, *35*, 3225.
(19) Laurer, J. H.; Hajduk, D. A.; Fung, J. C.; Sedat, J. W.; Smith, S. D.; Gruner, S. M.; Agard, D. A.; Spontak, R. J. *Macromolecules* **1997**, *30*, 3938.
(20) Spontak, R. J.; Fung, J. C.; Braunfeld, M. B.; Sedat, J. W.; Agard, D. A.; Kane, L.; Smith, S. D.; Satkowski, M. M.; Ashraf, A.; Hajduk, D. A.; Gruner, S. M. *Macromolecules* **1996**, *26*, 4494.
(21) Jinnai, H.; Nishikawa, Y.; Spontak, R. J.; Smith, S. D.; Agard, D. A.; Hashimoto, T. *Phy. Rev. Lett.* **2000**, *84*, 518.
(22) Furukawa, H.; Shimizu, M.; Suzuki, Y.; Nishioka, H. *JEOL News* **2001**, *36*, 12.
(23) Takahashi, K.; Hasegawa, H.; Hashimoto, T.; Bellas, V.; Iatrou, H.; Hadjichristidis, N. *Macromolecules* **2002**, *35*, 4859.
(24) Egerton, R. F. *Electron Energy-Loss Spectroscopy in the Electron Microscope*, 2nd ed.; Plenum: New York, 1996.
(25) Yamauchi, K.; Hasegawa, H.; Hashimoto, T.; Iwawaki, E.; Masuda, T. Manuscript in preparation.
(26) Frank, J., Ed. *Electron Tomography*; Plenum: New York, 1992.

MA034840K